PHILOSOPHICAL TRANSACTIONS OF THE ROYAL SOCIETY A

Phil. Trans. R. Soc. A (2006) **364**, 821–844
doi:10.1098/rsta.2006.1739
Published online 21 February 2006

Recent relative sea-level trends: an attempt to quantify the forcing factors

By Hans-Peter Plag*

Nevada Bureau of Mines and Geology, University of Nevada, Mailstop 178, Reno, NV 89557, USA

Local sea-level is affected by a number of forcing factors, which all contribute to the trends observed by tide gauges. Here we use the fingerprints of main factors contributing to secular sea-level trends to construct an initial empirical model that explains best the trends in sea-level as recorded by the large number of coastal tide gauges over the last 50 years. The forcing factors considered include steric changes derived from observations, post-glacial rebound as predicted by geophysical models and mass changes in the Greenland and Antarctic ice sheets as predicted by the static sea-level equation. The approximation of the observed spatial pattern of sea-level trends through a model based on the spatial fingerprints of the main forcing factors fully utilizes the information contents of the available observations and models and allows the interpolation of the sea-level trends between the tide gauges. As a result, we obtain the global picture of sea-level trends due to the forcing factors accounted for in the analysis. Moreover, we derive constraints on the mass changes of the large ice sheets.

The empirical models explain about 15% of the variance of the sea-level trends. Nevertheless, the models are correlated with the observations on the level of 0.38 ± 0.07, indicating that most of the unexplained variance is due to contributions with small spatial scales. Averaged over the last five decades, the results indicate that the Antarctic and Greenland ice sheets have been melting with an equivalent contribution to global sea-level rise of 0.39 ± 0.11 and 0.10 ± 0.05 mm yr^{-1}, respectively. The steric signal derived from observations is clearly identified in the sea-level trends and is found to be at a minimum of 0.2 mm yr^{-1}, with the most likely value being close to 0.35 mm yr^{-1}. The global tide gauge network, which covers only a small fraction of the ocean surface, appears to sense an average sea-level rise larger than the global average. Extrapolating the regression models to the global ocean and taking into account the uncertainties in the extrapolation results in a most likely global average of the order of 1.05 ± 0.75 mm yr^{-1}.

Keywords: relative sea-level trends; ice mass changes; steric sea-level changes; global sea-level trend

1. Introduction

The recent Intergovernmental Panel on Climate Change (IPCC) assessments (Houghton *et al.* 1996, 2001) summarize our knowledge of global change and

*hpplag@unr.edu

One contribution of 20 to a Theme Issue 'Sea level science'.

focus on establishing reliable uncertainty boundaries for key parameters. In the framework of these assessments, Warrick *et al.* (1996) and Church *et al.* (2001) emphasize the considerable uncertainties in the mass balance of the ocean and, in consequence, the global sea-level. In particular, the contribution of the large ice sheets to current sea-level changes is rather uncertain.

The global mass and volume of the ocean are two absolute[1] quantities characterizing the ocean as a reservoir in the global hydrological cycle. Changes in these quantities are directly related to changes in the hydrological cycle and therefore to climate change. Local sea-level, which is defined here as the (absolute) distance between the surface of the ocean and the surface of the solid Earth, describes how the volume of the ocean is distributed in a given topography of the Earth surface. This distribution depends on many different factors, such as the Earth's topography, the (time-variable) geoid, changes of the Earth's rotation, atmospheric circulation, heat and salinity distribution in the ocean, ocean circulation, past and present mass movements in the Earth system, the visco-elastic properties of the Earth's interior, sedimentation and even anthropogenic subsidence due to groundwater, gas or oil extraction. At coastal locations, local sea-level is measured relative to a benchmark on land and widely denoted as relative sea-level (RSL[2]). Sea-level can also be given relative to a coordinate system (e.g. a geocentric coordinate system) or a reference plane (e.g. a geoid model or the reference ellipsoid).

It is well known and widely accepted that the disintegration of the last great ice sheets produced a distinct spatial pattern, a fingerprint, in RSL, with rather different temporal characteristics of the RSL in the near, intermediate and far field of the load changes (e.g. Quinlan & Beaumont 1982; Lambeck 1993). Present-day changes in the cryosphere and the other terrestrial hydrological reservoirs can also be expected to produce a distinct spatial fingerprint, which should be present in records of the local RSL measured, for example, with tide gauges. Based on these fingerprints, RSL observations, in principle, can be inverted for mass changes in the terrestrial hydrosphere.

Nevertheless, over the last 30 years many studies of sea-level variations have focused on the determination of a global sea-level rise from coastal RSL observations obtained with tide gauges, as well as on the explanation of this scalar quantity through a mass balance equation (see Warrick *et al.* 1996; Church *et al.* 2001 for a review). Based on a unique dataset of monthly mean sea-levels provided by the Permanent Service for Mean Sea Level (PSMSL), the global trend has been estimated to be of the order of $+1$ to $+2.5\,\mathrm{mm\,yr^{-1}}$. This relatively wide range is mainly due to the selection criteria used by the different researchers to select subsets of tide gauges as well as the methodology to determine a global trend. Methods include simple arithmetic averages of selected subsets of tide gauges (e.g. Barnett 1984), use of geological data to separate the present-day trend from past geological contributions (Gornitz & Lebedeff 1987) and decontamination of local trends for the present-day post-glacial signal on the basis of geophysical models (e.g. Peltier & Tushingham 1991). Recently, Douglas (1991, 1997) selected a small number of tide gauges with long records in areas

[1] The adjective *absolute* is used for quantities that are not reference frame-dependent.

[2] We will keep the term *relative sea-level* despite the fact that sea-level given as the distance between sea surface and the surface of the solid Earth is a reference frame-independent and thus absolute quantity.

considered as tectonically stable and corrected the local trends for the post-glacial contribution. Based on the consistency of the local trends at these tide gauges, he then deduced that they represent the global trend.

The mainly arithmetic approach applied in all of these studies has been criticized by, for example, Pirazzoli (1989), Plag (1993) and Gröger & Plag (1993), who all pointed out that the large spatial variability of the local RSL trends inadvertently biases a global estimate. Plag (1993) even claimed that it is not possible to determine a global sea-level change from tide gauges due to their deficiencies in spatial sampling. However, Plag & Jüttner (2001) pointed out that utilizing fully the complex physical relationship between sea-level and ocean mass changes, the global network of tide gauges could well be sufficient to constrain the mass movements having contributed to the observed trends in local RSL.

Plag & Jüttner (2001) and Mitrovica *et al.* (2001) emphasized again the well-known fact that RSL changes caused by mass exchange of the ocean with the terrestrial hydrosphere and cryosphere will not be spatially homogeneous, a relation well described by the so-called sea-level equation derived by Farrell & Clark (1976). Any relocation of surface mass, such as the ice sheets, glaciers, ground water and oceans, loads and deforms the solid Earth and changes the Earth gravity field. The resulting geoid changes redistribute the mass in the ocean and thus affect local RSL. Moreover, RSL is also affected by vertical motion of the land due to the load-induced deformation of the solid Earth. As a consequence, any mass exchange between the ocean and the other reservoirs in the global water cycle is associated with a specific spatial fingerprint.

Likewise, sea-level changes due to variations in the heat content of the ocean have a distinct spatial pattern associated with them, depending on where the heat content is increased or decreased. Sea-level trends computed from oceanographic observations reflect this very clearly, showing spatial variations, which are at least an order of magnitude larger than the global averages (see §2).

RSL changes have been observed with coastal tide gauges at many locations for more than five decades and in some places for up to 200 years. However, the spatial distribution of tide gauges is far from being even. Moreover, the records cover different intervals and only for the last five decades has a nearly global coverage of at least the continental coast lines been achieved.

This study makes an attempt to approximate the spatial pattern of the observed local RSL trends through a model based on the spatial fingerprints of main forcing factors. Thus, we fully use the available observations and the models describing the global fingerprints of the forcing factors. This approach also allows the interpolation of the RSL trends between the tide gauges. As a result, we obtain the global picture of the RSL trends due to the forcing factors accounted for in the analysis. Moreover, we will be able to determine a truly global average not biased by the uneven distribution of the RSL observations.

In §2, we will first discuss the local RSL balance describing the observations as a sum of contributions originating from different forcing factors. Then, in §3, we will consider the available datasets for both the RSL observations and the forcing factors. In §4, a regression model is set up between the observed RSL trends and the available forcing factors, and the results of the regression analyses are presented in §5. Finally, the main conclusions as well as the open questions are summarized in §6.

2. Local sea-level balance

The RSL measured by a tide gauge is the result of a number of forcing factors acting on a wide range of spatial and temporal scales (e.g. Chelton & Enfield 1986). The factors include but are not limited to waves, tides, meteorological forcing, ocean currents, mass and heat changes of the ocean, geophysical processes affecting the land level and the geoid and human-made processes. Considering monthly mean sea-levels at a tide gauge located at a point $\vec{x}$ on the Earth surface, then the variations h in RSL can be approximated as a sum of several factors, namely

$$h(\vec{x},t) = S(\vec{x},t) + C(\vec{x},t) + A(\vec{x},t) + I(\vec{x},t) + G(\vec{x},t) + T(\vec{x},t) + P(\vec{x})(t-t_0) + V_0(\vec{x})(t-t_0) + \delta V(\vec{x},t), \tag{2.1}$$

where t is time and t_0 an arbitrary time origin. The balance considers the following processes: S, steric changes; C, changes in ocean currents; A, changes in atmospheric circulation; I, changes in the mass of large ice sheets; G, changes in the mass of glaciers; T, changes in the terrestrial hydrosphere; P, post-glacial rebound; V_0, tectonic vertical land motion; δV, nonlinear vertical land motion. However, considering only those factors that contribute to secular trends with a fingerprint exhibiting large spatial variations on long to global scales, we are left with the post-glacial rebound signal (PGS), the steric signal and the contribution from the two large ice sheets in Antarctica and Greenland. The database and RSL fingerprint functions for these factors are discussed in §3.

Potentially, changes in the atmospheric circulation might induce ocean current changes. Secular variations in the spatial pattern of the mean air pressure field introduce secular changes in sea-level due to the inverted barometer (IB) response of the ocean. An analysis of the ERA40 air pressure field available from the European Center for Medium Range Weather Forecast showed that over a time window of nearly 50 years, the maximum secular trends are found to be of the order of $0.01\,\mathrm{HPa\,yr^{-1}}$ (Plag *et al.* 2005), which is equivalent to $0.1\,\mathrm{mm\,yr^{-1}}$ in IB response. Changes in the mean wind field can result in changes of sea-level particularly at coastal sites. These changes will have small spatial scales due to a complex interplay of the wind field and the coastal geometry. Here, we assume that these contributions are negligible compared to the main factors mentioned above. Contributions from changes in continental glaciers result mainly from mass changes in small-scale sources distributed over the global land area. Global models are available (e.g. Meier 1984), but there are considerable deficiencies in global coverage and mass balance of individual glaciers (see Church *et al.* 2001 for a detailed discussion). The resulting RSL fingerprint will be dominated by small spatial scales in the near-field of the individual glaciers and fairly constant amplitudes over most of the ocean surface.

Changes in the mass balance of the continental hydrosphere are expected to contribute to global sea-level trends on the level of $0.5\,\mathrm{mm\,yr^{-1}}$ (see Church *et al.* 2001 and references therein). The sea-level fingerprint due to these changes is expected to be dominated by small spatial wavelength in the vicinity of the coasts and nearly constant amplitudes in the far-field. The only exception may be due to trends in the average snow load, thawing of permafrost and regional

deforestation, which may induce considerable large-scale patterns. Currently, there is no sufficient model available to account for these contributions comprehensively. Consequently, we have to neglect the fingerprints of glaciers and the continental hydrosphere. Large parts of the ocean's coasts are in deformation areas associated with plate tectonics and experience vertical land motion on spatial scales from 30 to 100 km (e.g. Emery & Aubrey 1991) at the lower end to the size of the plates at the high end. Currently, no global model or observational database exists that would allow the derivation of the resulting RSL fingerprint. This study aims at large spatial scales, and therefore the secular tectonic signal is considered as noise. The same is true for nonlinear vertical land movements due to plate-boundary processes or anthropogenically induced, except for co-seismic displacements, which are partly eliminated from the RSL observations (see §3).

3. The database

The PSMSL has collected a major fraction of the global tide gauge data and provides a dataset of records of monthly mean RSL for more than 1950 tide gauges (see Woodworth & Player 2003 for a description of the PSMSL and its dataset). The PSMSL carries out a detailed error check of the data (Woodworth *et al.* 1990) and those records for which the history of a local reference can be established are compiled into a subset denoted as Revised Local Reference (RLR) dataset. Only the records of the RLR subset can be used confidently to determine local RSL trends.

The signal content of the monthly mean sea-level records depends strongly on the geographical location. However, at most locations, a large seasonal signal is present while secular trends mostly fall into the interval of $\pm 10\,\mathrm{mm\,yr^{-1}}$. Moreover, most records show interannual to multidecadal variations of the order of a few millimetres to tens of millimetres, which can be attributed to internal ocean processes and atmospheric forcing. These variations can bias trends determined from records of less than several decades. Therefore, it is crucial that the secular trends for the RSL observations and the forcing factors are representative for the same time window.

A few of the records provided by the PSMSL have a length of more than 100 years, but most of the records are restricted to the time window of approximately 1950–2000. Therefore, we can only expect to have a spatially sufficient picture of the pattern of RSL trends in that time interval. Considering that the steric sea-level heights are given for the time window 1950–1998 (see table 1), we choose this time window as a compromise between highest accuracy for the local secular RSL trends and the optimal spatial coverage. For each RSL record, a secular trend is determined by fitting the model function,

$$g(t) = A_{\mathrm{A}} \sin(\omega_{\mathrm{A}} t + \phi_{\mathrm{A}}) + A_{\mathrm{SA}} \sin(\omega_{\mathrm{SA}} t + \phi_{\mathrm{SA}}) + a + bt, \tag{3.1}$$

to the series of monthly sea-levels, where t is time, A and φ are the amplitude and phase, respectively, of an annual (index A) and semiannual (index SA) constituent, a is an offset and b the constant secular RSL trend. Trends have also been determined using an extended version of equation (3.1), which included a nodal tide (period 18.6 years), a constituent representing the solar sunspot

Table 1. Datasets for thermosteric sea-level variations. (All thermosteric sea-level heights were provided by A. Cazenave (2002, 2003, personal communication). N is the number of grid cells. A is the surface of the grid in percentage of the total Earth surface. See Lombard *et al.* (2005) for details of the computation of the steric sea-level heights.)

symbol	oceanographic data	depth	temporal resolution	N	A
I500	Ishii *et al.* (2003)	500 m	1 year	40 779	68.08
L500	Levitus *et al.* (2000)	3000 m	1 year	41 191	68.56
L3000	Levitus *et al.* (2000)	500 m	1 month	41 163	68.51

cycle (period approx. 10.0 years) and a pole tide (period 1.18 years). Only the trend values for shorter records are affected by this extension, while the results reported in §5 do not change significantly.

Thermosteric sea-level variations can be computed from observations of the subsurface temperature field. Currently, two global datasets are available, namely Levitus *et al.* (2000) and Ishii *et al.* (2003) with a temporal resolution of 1 year and 1 month, respectively. Both datasets have spatial resolution of 1° in longitude and latitude. The former is given for the interval 1945–1998 and the latter for the interval 1950–1998. The two datasets are, to a large extent, based on the same observations; however, different analysis schemes are used to create the gridded datasets. The sea-level trends derived from these two datasets display considerable differences (figure 1), with the former having more short wavelength variations and a larger range of local trends. The differences in the two datasets are studied in detail by e.g. Lombard *et al.* (2005). They point out that for the 1990s, the Levitus *et al.* (2000) dataset shows a global trend nearly three times larger than the Ishii *et al.* (2003) data, and attribute this to errors in the processing. Moreover, according to them, the I500 dataset is likely to underestimate the thermosteric contribution due to an omission of expendable bathythermograph (XBT) depth correction.

Here, we will use sea-level heights derived from both datasets in order to determine which of the two sets results in a better approximation of the observed pattern in RSL trends. For that, we use the three sea-level height datasets described in table 1. For the steric sea-level heights denoted as L500 and L3000, which are given as annual means, local trends are determined by a least-squares fit of a polynomial of degree 1 to the data for each grid point. I500 is given as monthly means, and the model function (3.1) is fitted to the time-series for each grid point in order to determine the local trends. Using a depth of only 500 m for the computation of thermosteric sea-level variations can be expected to be biased over a large area of the ocean, where the thermocline depth is deeper. However, most tide gauges are at coastal locations, and there the datasets using a 500 m depth may well be more representative than the L3000 dataset.

The uncertainties in the mass changes of the two largest ice sheets, namely Antarctica and Greenland, over the last five decades are too large to base the RSL fingerprints of these ice sheets on observations. Therefore, Plag & Jüttner (2001) determined for each ice sheet a fingerprint function for a constant, unit trend over the complete area of the ice sheet. These fingerprints were determined by solving the static sea-level equation derived by Farrell & Clark (1976). For time scales of up to a century, the sea-level equation can be treated elastically, and in this case,

the equation can be solved analytically, resulting in the fingerprints shown in figure 2. The Antarctic fingerprint has a distinct zonal component, while the Greenland fingerprint shows more variations with longitude, particularly in the Northern Hemisphere. Plag & Jüttner (2001) also determined the fingerprint for an average mass change in the ice cover of Iceland. However, this fingerprint is found to be highly correlated with the Greenland fingerprint and cannot be distinguished from the latter one on the basis of the RSL observations available.

As mentioned in §2, geophysical models predict the present-day RSL fingerprint of the PGS fairly well (for a review, see Peltier 1998). In order to estimate the effect of the uncertainties of the predicted PGS fingerprint in RSL, we have used a suite of models in the regression analysis (table 2). In figure 3, two PGS predictions are compared. Both predictions display maximum negative contributions close to the centres of the former ice loads in Fenoscandia and North America. However, there are also marked differences, which are solely due to different solid Earth models used for the two examples. Largest differences are found in the Arctic and around Antarctica. Thus, it can be expected that the correlation between the post-glacial RSL fingerprints and those of the other factors, particularly those of the ice sheets, display some variety depending on the prediction used for the PGS.

4. The regression model

Ideally, we would base an appropriately parameterized regression model on the complete version of equation (2.1). However, since we do not have sufficient observations and/or model predictions for all forcing factors, we have to restrict the regression model to the main factors, for which fingerprints are available. Moreover, we will restrict the model to RSL trends. Based on the discussion in §§2 and 3, this leads to the regression equation

$$\tilde{b}_i = \sum_{j=1}^{K} \alpha_j I_i^{(j)} + \beta P_i + \gamma S_i + c, \tag{4.1}$$

where $\tilde{b}_i$ is the modelled RSL trend at tide gauge i, $I_i^{(j)}$ the RSL trend at tide gauge i due to a unit mass change in ice sheet $I^{(j)}$, K the number of individual ice sheet fingerprints included in the regression, P_i the predicted PGS at tide gauge i, S_i the thermosteric RSL trend at tide gauge i derived from a gridded thermosteric dataset and c a mean global RSL trend introduced to collect all unaccounted contributions.

The α_j are unknown mean mass trends of the ice sheets, which are determined as a results of the regression analysis. β is introduced to account for any scale error in the PGS predictions. With the introduction of β, we preserve the predicted PGS fingerprint, but we allow for adjustments in the amplitude. The same is true for the thermosteric effect, where we have introduced a scale factor γ.

A complication arises from the fact that the thermosteric contribution is only given on a 1° by 1° grid. Using equation (4.1) directly would require interpolation and, in most cases, extrapolation of the steric signal from nearby grid points to the exact tide gauge location. Alternatively, the local RSL trends can be used to create a gridded dataset of the RSL trends. For the geophysical models, both

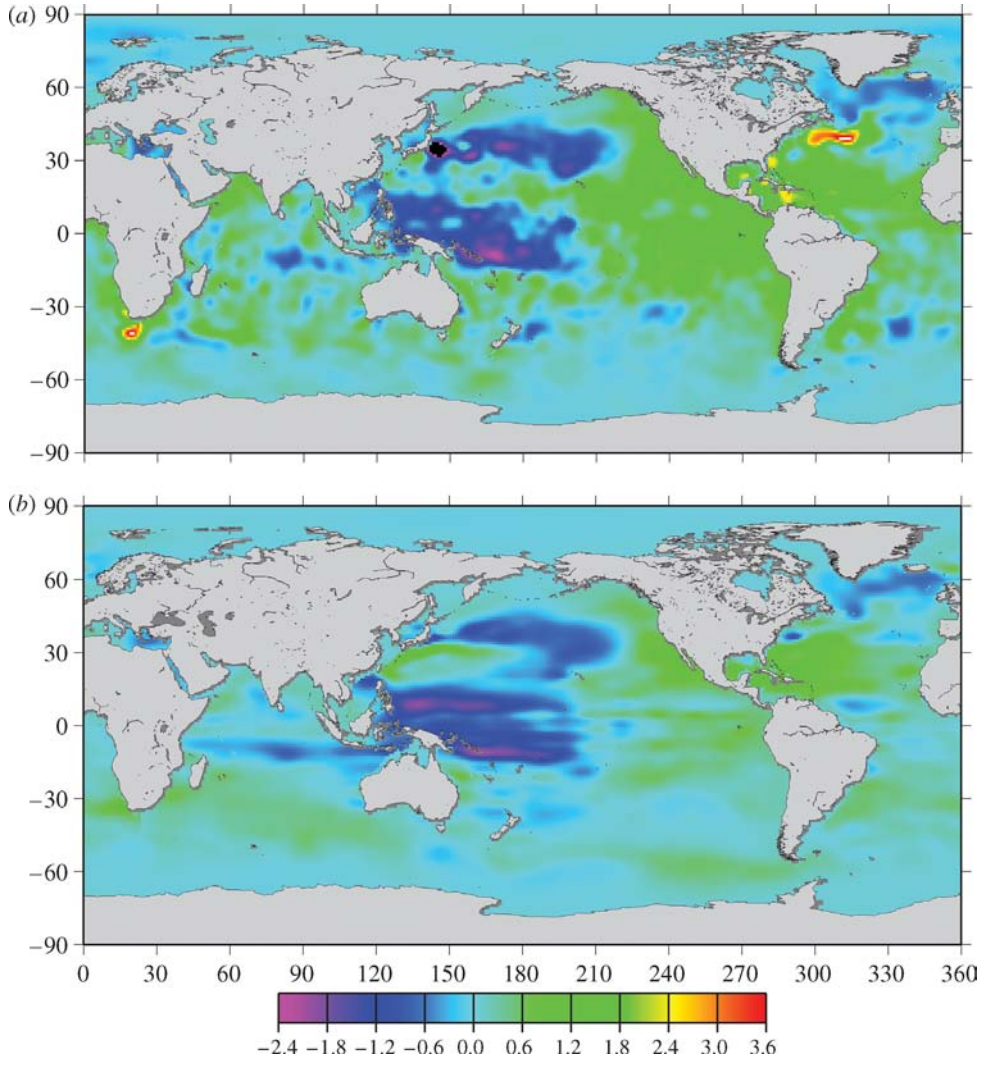

Figure 1. Spatial fingerprint of the thermosteric sea-level trend for the interval 1950–1998. (*a*) Trends for L500; (*b*) trends for the I500.

alternatives are equally feasible, since the models can be computed for an exact tide gauge location or averaged over a grid cell.

A detailed sensitivity study showed that for the first alternative, the results of the regression strongly depends on the data filter used to exclude certain tide gauges, for example, on the basis of the record length being to short or the trend value being outside an interval. Therefore, here we use the second alternative.

In figure 4, the complete grid of sea-level trends determined from the RLR-records covering most of the interval 1950–1998 is shown. In the computation of the grid values, local RSL trends outside of $\pm 12\ \mathrm{mm\ yr^{-1}}$ were rejected and so were records shorter than 10 years. The RSL trends in a grid cell were averaged using the length of the records as weights. As expected from the distribution of

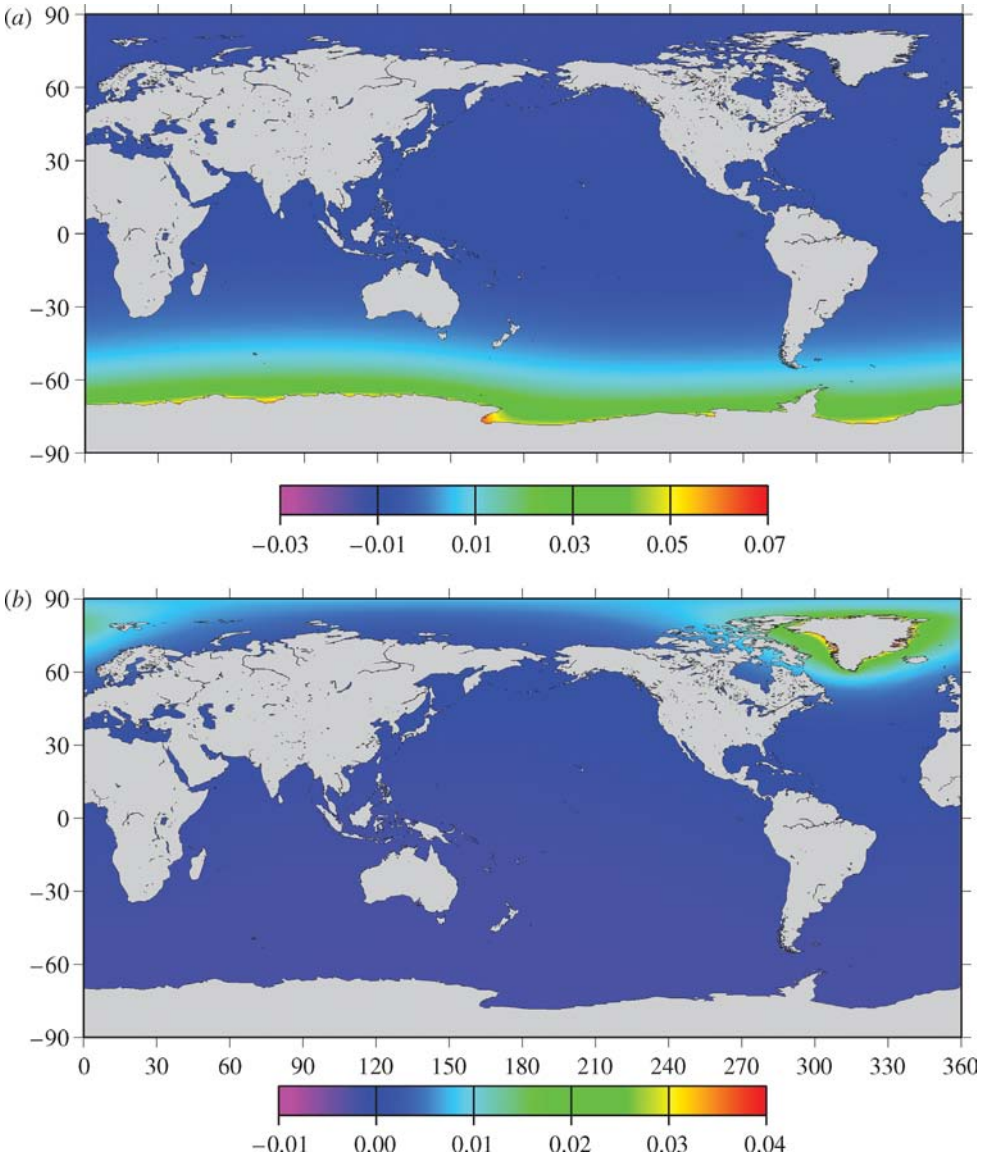

Figure 2. Spatial fingerprints of changes in the mass of the large ice sheets in RSL trends. (*a*) Fingerprint of the Antarctic ice sheet; (*b*) fingerprint of the Greenland ice sheet. The fingerprints are based on a solution of the static sea-level equation for degree and order 72. The fingerprints are given for a unit mass change.

tide gauges, the best spatial coverage is found for the coasts of the Northern Hemisphere and the open equatorial Pacific, while on the Southern Hemisphere, coverage is generally sparse.

Similar grids are created for all available forcing factors. For all factors, the 1° grids are averaged to form the grids with lower resolution. Thus, for the regression, a modified version of equation (4.1) is used, where the index i denotes the grid cell instead of the tide gauge.

Table 2. Predictions of the present-day RSL fingerprint due to post-glacial rebound. (Predictions are from J. X. Mitrovica (1999, 2001, personal communication). N_0 is the cut-off degree for spherical harmonic expansion; d is the lithospheric thickness in units of km; η_u is the upper mantle viscosity in units of 10^{21} Pa s; η_l is the lower mantle viscosity in units of 10^{21} Pa s. Ice history is for all predictions according to ICE-3G. For details on the computation see Milne *et al.* (1999).)

N	model	N_0	d	η_u	η_l
P1	120_1_2	256	120	1.00	2.00
P2	120_1_475	256	120	1.00	4.75
P3	12011.mn	128	120	1.00	1.00
P4	12012.mn	128	120	1.00	2.00
P5	12015.mn	128	120	1.00	5.00
P6	120110.mn	128	120	1.00	10.00
P7	120p32.mn	128	120	0.30	2.00
P8	120p52.mn	128	120	0.50	2.00
P9	7112.mn	128	71	1.00	2.00
P10	9612.mn	128	96	1.00	2.00

In the following, we will distinguish between the *regression grid*, which is defined by the fact that all factors used in a regression are available, and the *complete grid*, which is defined through the grid points given for a specific forcing factor or the observed RSL trends. Since all PGS predictions and Greenland and Antarctic loading models are available globally, the regression grids are determined as the set of grid cells where both the steric sea-level trends and the observed RSL trends are given. Table 3 summarizes the main characteristics of the regression and complete grids as functions of resolution. Using a resolution of 1° results in only a low number of grid cells common for the complete RSL and steric grids. For lower resolutions, the short spatial scales, particularly in the steric datasets, are reduced, as is indicated by the consistently lower variance for the low-resolution grids of the thermosteric sea-level trends. Furthermore, with respect to the spatial resolution of the grid, the sensitivity study showed that a grid spacing of 2° in longitude and latitude appears to be a good compromise between spatial resolution and the insensitivity of the solution to pre-selection of tide gauges based on the data filter. The discussion of the regression results in §5 is therefore mainly based on the grids with resolution of 2°.

Table 3 also elucidates the large differences of the average trends in thermosteric sea-levels predicted by the three different steric datasets. With the exception of the grids with a resolution of 1°, the averages on the regression and complete grids are rather similar for each steric dataset. This indicates that for these resolutions the average steric signals on the regression grids are close to the global signal. It is pointed out here that the global averages for the I500 and L500 dataset agree with those reported in Lombard *et al.* (2005).

For the observed RSL, the regression grid has its largest average trend of 1.16 mm yr^{-1} for a resolution of 2°. Taking the complete observation grid, the maximum average trend of 1.07 mm yr^{-1} is found for a resolution of 1°. These values are averages of the local sea-level trends over a grid covering only about 3.1 and 1.6%, respectively, of the ocean surface. Therefore, they cannot be

compared to global sea-level trends obtained by, for example, Douglas (1997) through a selection of tide gauges with long records.

Any regression analysis is hampered by the presence of high covariance of the forcing factors. In order to study the covariance of the factors, we consider the cross-correlation matrix given in table 4. The spatial correlation coefficient ρ for two fields g and h, which are functions of two coordinates x and y and which are given on the same grid points (i.e. given as g_{ij} and h_{ij}, $i=1, \ldots, n_x$, $j=1, \ldots, n_y$) is defined as

$$\rho = \frac{\sum_{i=1}^{n_x}\sum_{j=1}^{n_y} v_{ij} g_{ij} h_{ij}}{\sqrt{\sum_{i=1}^{n_x}\sum_{j=1}^{n_y} v_{ij} g_{ij}^2 \sum_{i=1}^{n_x}\sum_{j=1}^{n_y} v_{ij} h_{ij}^2}}, \tag{4.2}$$

with v_{ij} being the area of the grid cell pertaining to the point with indices ij.

The correlation coefficients computed for the regression grids indicate that several forcing factors are significantly inter-correlated on that grid. In particular, the fingerprints of the Antarctic and Greenland ice sheet are significantly anti-correlated. Moreover, the Greenland ice sheet fingerprint has a weak correlation with the present-day PGS fingerprint.

The different PGS fingerprints are correlated with each other on the level of 0.9 or more (not included in table 4), indicating that over most of the regression grids, these models are in reasonable agreement. For the steric fingerprints, the correlation between I500 and L500 is 0.83 on the regression grid, while the correlation for the complete set of common grid points amounts to only 0.73. Thus, there are considerable differences between these two models, though the regression grid does not capture all of these differences. The L3000 fingerprint appears to be rather different from both the L500 and I500 fingerprints, both on the regression grid and the complete grids.

It should be mentioned here, however, that since the PGS is closely correlated with the signal of present-day changes in ice masses, any errors in the PGS will bias the estimates of these present-day changes. Moreover, the anti-correlation of the Antarctic and Greenland fingerprints combined with the fact that most of the regression grid cells are on the Northern Hemisphere can be expected to bias the regression result, particularly for the Antarctic fingerprint. Computing for all PGS predictions the correlation coefficients with the other factors reveals the following: (i) the fingerprints of all PGS predictions are clearly correlated with the spatial pattern of the observed RSL trends, with the correlation coefficient being of the order of 0.22 (for P3) to 0.38 (for P5). (ii) The highest correlation between the PGS fingerprints and the other factors is found for the Greenland ice sheets, with the highest correlation coefficient being 0.31 (for P7). This result indicates that the regression coefficient α_{G} for Greenland can be expected to depend on the PGS prediction used in the regression. (iii) Most of the PGS fingerprints are not correlated with any of the three steric fingerprints, with the exception of P6, where a barely significant correlation of approximately 0.15 is found.

The weighting of the observations in the regression analysis deserves special attention. Intuitively, a weighting by area of the individual grid cells appears appropriate. However, each occupied grid cell is based on the weighted mean of

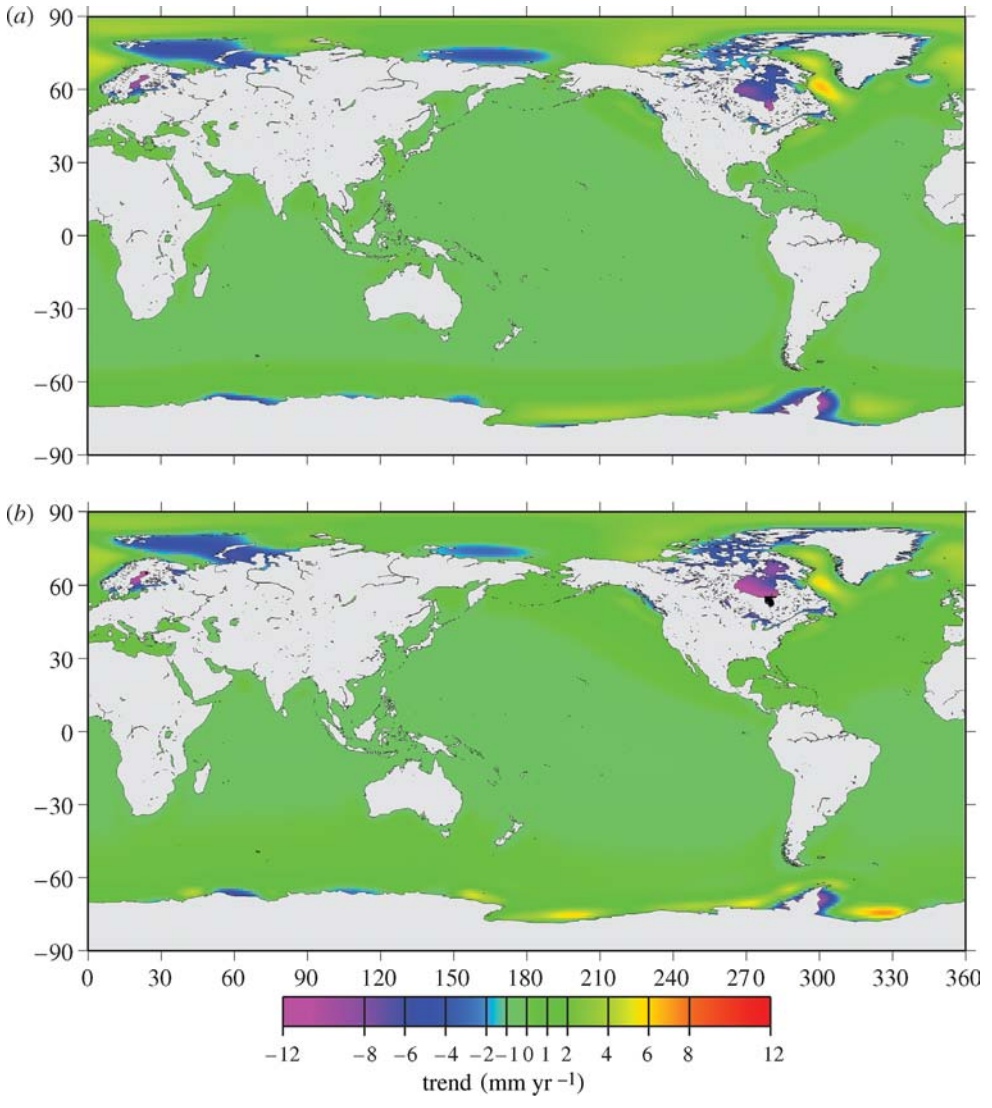

Figure 3. Spatial fingerprint of the present-day post-glacial signal in sea-level trends. (*a*) Predictions based on model P1; (*b*) model P6, see table 2.

one or more local RSL trends, where the weight is the length of the RSL record. Introducing additional weighting of the grid cells by their area reduces the importance of high-latitude grids relative to those near to the equator. This is equivalent to reducing the weights of the cells closer to Antarctica and Greenland. Test computations showed that areal weighting results in considerably larger uncertainties for the regression coefficients of the Antarctic and Greenland fingerprints, while those for the PGS and steric signals remain nearly the same. Moreover, using areal weighting, the regression coefficient for the Greenland fingerprint is in most cases not significant on the 95% level. Therefore, areal weighting is not applied in the regression. However, a weight of

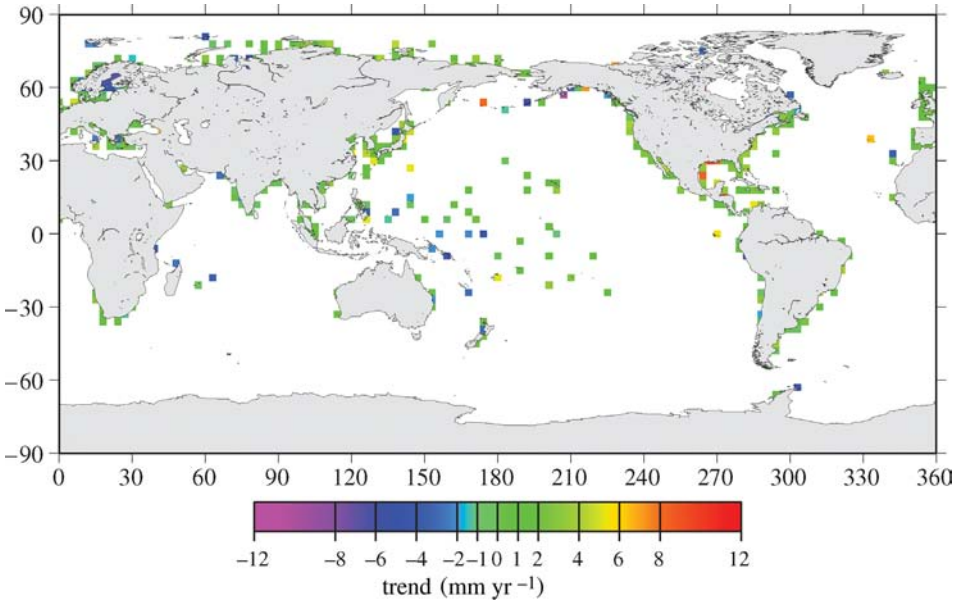

Figure 4. Spatial pattern of the sea-level trend in the period 1950–1998. The grid cells are those of the 2°×2° grid in table 3. For better visibility, the grid cells have been plotted as 3°×3°cells.

the individual observation grid cells based on the accuracy of the sea-level trend assigned to the cell can be expected to reduce the spreading in the results discussed in §5.

5. Results

We will first consider the sensitivity of the regression results with respect to the grid resolution and the PGS prediction used. After that, we will discuss selected results for different model compositions. In the following, all error estimates are confidence intervals for the 95% level computed from the full covariance matrix of the least-squares fit of equation (3.1) or a truncated version to the observations on the regression grid.

A major advantage of the fingerprint methodology is the ability to extrapolate the results obtained for the regression grid to the complete steric grid, which is close to the global ocean surface. The necessary assumption is that the fingerprints are globally of the same quality and accuracy as they are for the regression grid. Under this assumption, which is easy to justify for the ice mass fingerprints and the PGS, but less obvious for the steric sea-levels, the methodology allows the computation of the individual contribution for the complete steric grids. Therefore, we discuss both the individual contributions on the regression grid and the complete grid.

The effect of grid resolution on the regression is demonstrated in table 5 for a model based on the PGS prediction P2 and the steric heights I500. Any other choice for these two factors results in a similar dependency of the regression results on grid resolution. For each solution, the estimated parameters are given

Table 3. Parameters of complete grids of RSL and steric forcing factor as well as of the resulting regression grids. (R is the resolution of the grid; N is the number of grid cells occupied; A is the area in percentage of the global ocean surface; E is the areally weighted mean of the respective parameter in mm yr^{-1}; σ is the standard deviation of the parameter in mm yr^{-1}. The last two columns give E and σ for the RSL trends on the regression grids. Datasets are as given in tables 1 and 2.)

		complete grids				regression grids					
						factor				RSL	
R	grid	N	A	E	σ	N	A	E	σ	E	σ
1°	RLR	642	1.58	1.07	2.97						
	I500	40 779	96.29	0.05	0.38	121	0.33	−0.06	0.63	1.04	2.58
	L500	41 191	96.98	0.21	0.46	132	0.35	0.09	0.59	1.07	2.51
	L3000	41 163	96.91	0.35	0.95	132	0.35	0.16	1.03	1.07	2.51
2°	RLR	489	4.86	1.01	2.86						
	I500	10 722	100.88	0.05	0.37	284	2.97	0.07	0.48	1.09	2.78
	L500	10 865	101.85	0.21	0.45	303	3.14	0.21	0.54	1.16	2.78
	L3000	10 854	101.73	0.34	0.92	301	3.12	0.35	0.93	1.12	2.76
3°	RLR	406	9.13	0.98	2.72						
	I500	4976	104.99	0.05	0.36	330	7.63	0.08	0.45	1.01	2.62
	L500	5059	106.17	0.21	0.45	343	7.88	0.25	0.54	1.02	2.65
	L3000	5054	106.06	0.34	0.90	340	7.81	0.36	0.95	0.99	2.65
5°	RLR	287	18.01	0.89	2.78						
	I500	1891	110.05	0.05	0.35	251	16.16	0.06	0.47	0.86	2.67
	L500	1922	111.41	0.21	0.43	256	16.47	0.24	0.58	0.91	2.67
	L3000	1920	111.28	0.33	0.85	254	16.33	0.36	0.99	0.88	2.65
10°	RLR	167	42.64	0.75	2.67						
	I500	518	120.25	0.06	0.31	158	40.89	0.05	0.40	0.75	2.59
	L500	532	122.87	0.21	0.39	163	41.90	0.23	0.49	0.74	2.62
	L3000	532	122.87	0.33	0.72	163	41.90	0.35	0.87	0.74	2.62

in equivalent contribution to the mean over the regression grid as well as the mean over the complete grid.

For a resolution of 1°, the number of grid cells is small and their distribution in space is rather uneven so that the regression results for the two ice sheets are barely significant. For resolutions of 2° and 3°, the regression detects the fingerprints of the two ice sheets. For the Greenland ice sheets, the results are significant on a 95% level but not on a 98% level. For Antarctica, the results are significant on the 98% level but the results depend strongly on the grid resolution. Moreover, in an F-test of the statistical significance of the models given in table 5, only the results for the resolutions of 2° and 3° are marginally significant.

For all resolutions, the PGS is well determined by the observations. However, the contribution of the PGS to the average on the regression grid depends on the grid resolution. The average over the complete grid is close to the theoretical value for the global ocean surface, i.e. zero, with the small non-zero values being due to the somewhat incomplete ocean coverage of the steric grids. The steric

Table 4. Correlation matrix for the fingerprints of the forcing factors and RSL. (Columns are: A and G: fingerprints of the Antarctic and Greenland ice sheets, respectively; P1: post-glacial rebound model, see table 2; I500, L500, L3000: thermosteric fingerprints, see table 1; and RSL: RSL trend pattern. Upper matrix is for cross-correlation on the regression grid (see table 3 for the number of grid cells), while lower matrix is for the complete grid defined by each pair.)

	A	G	P1	I500	L500	L3000	RSL
A	1.000	−0.492	−0.118	−0.026	−0.004	−0.120	−0.097
G	−0.492	1.000	−0.187	0.100	−0.023	−0.001	−0.074
P1	−0.118	−0.187	1.000	0.014	−0.006	0.023	0.317
I500	−0.026	0.100	0.014	1.000	0.826	0.675	0.248
L500	−0.004	−0.023	−0.006	0.826	1.000	0.832	0.247
L3000	−0.120	−0.001	0.023	0.675	0.832	1.000	0.186
RSL	−0.097	−0.074	0.317	0.248	0.247	0.186	1.000
A	1.000	−0.327	0.140	0.068	−0.090	−0.056	−0.119
G	−0.327	1.000	0.193	0.004	−0.038	−0.045	0.002
P1	0.140	0.193	1.000	0.014	−0.025	−0.019	0.195
I500	0.068	0.004	0.014	1.000	0.739	0.567	0.248
L500	−0.090	−0.038	−0.025	0.739	1.000	0.774	0.247
L3000	−0.056	−0.045	−0.019	0.567	0.774	1.000	0.186
RSL	−0.119	0.002	0.195	0.248	0.247	0.186	1.000

signal is also significantly detected with a contribution to the averages on the regression and complete grid depending only weakly on the grid resolution.

For all resolutions and all factors except the steric changes, there are large differences between the contributions on the regression and complete grids, respectively. This demonstrates that for each factor the tide gauge network only senses a strongly biased signal. Moreover, the average trends as seen by the regression grids are different from the averages on the complete grids. Thus, the tide gauge network only senses a rather biased global trend.

As pointed out in §4, the solutions for a grid resolution of 2° are those most insensitive to the selection of tide gauges. Therefore, in the following, only results for a resolution of 2° are discussed.

In the extrapolation of the regression results to the complete grid, we have assumed that the constant c remains unchanged. This is only justified if there are no other contributions with large spatial variation, which could be sampled by the tide gauge network with a large bias. Any such contribution would bias the extrapolation to the same extent.

The dependency of the regression results on the choice of the PGS model is illustrated in tables 6 and 7. Table 6 gives the regression results for the full model using the I500 steric dataset and 2° grid resolution for all different PGS predictions. The values in this table are given in equivalent contribution to the average. The contribution from the steric model is nearly unaffected by the choice of the PGS prediction. The higher covariance of the fingerprints of the two ice sheets and the PGS (see table 4) results in considerable variations of the regression results for the two ice sheets, depending on the post-glacial model selected. For all models, the PGS seen by the regression grid is negative, i.e. the effect of land uplift is dominant on the regression grid. In all cases, the two ice

Table 5. Dependency of regression results on grid resolution. (The model used for all resolutions consists of $\tilde{b}_i = \alpha_A I_i^{(A)} + \alpha_G I_i^{(G)} + \beta P_i^{(P2)} + \gamma S_i^{(I500)} + c$. RSL trends are for the 1950–1998 window. Columns are as follows: R, resolution in degrees; N, number of grid cells used; E_{mod}, mean of modelled RSL trends (weighted by area); V, fraction of the variance in percentage explained by the regression model. For each resolution, the upper and lower lines give the regression coefficients in mm yr^{-1} equivalent contribution to the mean over the (small) regression grid and the (near-global) complete steric grids, respectively. The contributions are given with 95% confidence limits.)

R	N	α_A	α_G	β	γ	c	E_{mod}	V
1	121	1.24±1.04	0.00±0.08	−0.08±0.02	−0.07±0.02	−0.02±1.10	1.07	15.33
		0.53±0.44	−0.01±0.06	−0.03±0.01	0.05±0.01	−0.02±1.10	0.53	
2	284	0.61±0.37	0.04±0.03	−0.09±0.02	0.08±0.02	0.46±0.40	1.10	13.10
		0.27±0.16	0.09±0.07	−0.04±0.01	0.06±0.02	0.46±0.40	0.83	
3	330	0.49±0.30	0.03±0.02	−0.13±0.02	0.08±0.02	0.60±0.33	1.06	13.33
		0.22±0.13	0.06±0.04	−0.06±0.01	0.05±0.01	0.60±0.33	0.86	
5	251	0.28±0.31	0.03±0.03	−0.17±0.03	0.06±0.02	0.71±0.36	0.91	12.64
		0.13±0.14	0.05±0.05	−0.08±0.01	0.05±0.02	0.71±0.36	0.86	
10	158	0.59±0.34	0.05±0.04	−0.15±0.04	0.05±0.02	0.23±0.40	0.78	10.20
		0.27±0.16	0.06±0.05	−0.09±0.02	0.06±0.02	0.23±0.40	0.54	

Table 6. Dependency of regression results on post-glacial rebound model. (The model is the same as in table 5, except for the PGS model indicated in column M. Grid resolution is 2° and the number of cells in the regression grid is 284. The symbols used to denote the columns are the same as in table 5, and for each regression model, the two lines have the same meaning as explained in that table. All quantities are in mm yr^{-1}, except for V, which is in %.)

model	α_A	α_G	β	γ	c	E_{mod}	V
P1	0.69±0.37	0.06±0.03	−0.07±0.02	0.09±0.02	0.33±0.40	1.10	12.21
	0.31±0.17	0.13±0.07	−0.03±0.01	0.06±0.01	0.33±0.40	0.79	
P2	0.61±0.37	0.04±0.03	−0.09±0.02	0.08±0.02	0.46±0.40	1.10	13.10
	0.27±0.16	0.09±0.07	−0.04±0.01	0.06±0.02	0.46±0.40	0.83	
P3	1.18±0.35	0.09±0.03	−0.04±0.01	0.09±0.02	−0.23±0.38	1.10	11.67
	0.53±0.16	0.19±0.06	−0.02±0.01	0.06±0.01	−0.23±0.38	0.53	
P4	1.09±0.35	0.08±0.03	−0.08±0.02	0.09±0.02	−0.07±0.38	1.10	12.22
	0.48±0.15	0.16±0.06	−0.03±0.01	0.06±0.01	−0.07±0.38	0.60	
P5	0.95±0.36	0.06±0.03	−0.11±0.02	0.08±0.02	0.12±0.38	1.10	13.24
	0.42±0.16	0.12±0.06	−0.04±0.01	0.05±0.01	0.12±0.38	0.67	
P6	0.92±0.36	0.06±0.03	−0.10±0.02	0.08±0.02	0.14±0.38	1.10	13.28
	0.41±0.16	0.12±0.06	−0.04±0.01	0.05±0.01	0.14±0.38	0.68	
P7	1.16±0.35	0.04±0.03	−0.19±0.04	0.08±0.02	0.01±0.38	1.10	12.89
	0.52±0.16	0.09±0.06	−0.06±0.01	0.06±0.01	0.01±0.38	0.61	
P8	1.12±0.35	0.07±0.03	−0.12±0.03	0.08±0.02	−0.04±0.38	1.11	12.60
	0.50±0.16	0.14±0.06	−0.04±0.01	0.06±0.01	−0.04±0.38	0.61	
P9	1.11±0.35	0.08±0.03	−0.05±0.01	0.09±0.02	−0.13±0.38	1.10	11.87
	0.49±0.15	0.17±0.06	−0.03±0.01	0.06±0.01	−0.13±0.38	0.57	
P10	1.11±0.35	0.08±0.03	−0.07±0.02	0.09±0.02	−0.11±0.38	1.10	12.03
	0.49±0.16	0.17±0.06	−0.03±0.01	0.06±0.01	−0.11±0.38	0.58	

Table 7. Regression coefficients for PGS models and steric sea-level heights. (All regression coefficients are dimensionless and ideal values would be 1.0.)

	no steric	I500		L500		L3000	
model	β	β	γ	β	γ	β	γ
A,G,S			1.29±0.25		1.04±0.22		0.44±0.13
A,G,P1	0.63±0.06	0.44±0.10	1.26±0.25	0.50±0.09	1.04±0.22	0.50±0.09	0.44±0.13
A,G,P2	0.61±0.05	0.43±0.08	1.16±0.25	0.49±0.08	0.96±0.22	0.49±0.08	0.40±0.13
A,G,P7	1.93±0.15	1.35±0.26	1.18±0.25	1.53±0.25	0.97±0.22	1.50±0.25	0.37±0.13
A,G,P8	1.07±0.09	0.77±0.16	1.20±0.25	0.86±0.15	0.98±0.22	0.85±0.15	0.39±0.13
G,P1	1.20±0.10	0.49±0.09	1.25±0.25	0.54±0.09	1.05±0.22	0.53±0.09	0.46±0.12
G,P7	1.42±0.10	1.33±0.26	1.17±0.25	1.51±0.25	1.00±0.22	1.47±0.25	0.42±0.13

sheets contribute positively to sea-level rise, i.e. they are melting. For all models, Antarctica has a contribution to the average on the regression grid and complete grids equal to or larger than 0.61 and 0.27 mm yr^{-1}, respectively. For the Greenland ice sheet, these values are 0.04 and 0.09 mm yr^{-1}, respectively. It is worthwhile to note that the ratio of the contributions on the regression and complete grids is close to 2 for Antarctica and less than 0.5 for Greenland. The big difference in the two ratios is due to the main bulk of the cells in the regression grid being closer to Greenland, where the effect of the solid Earth's elastic response to the deloading of Greenland dominates that signal, and further away from Antarctica, where the sea-level rise due to mass added to the ocean is dominant.

The constant c in the regression analysis appears to depend strongly on the PGS prediction used and is anticorrelated with the regression coefficient for the Antarctic fingerprint. For most results in table 6, the remaining unexplained global average is less than 0.15 mm yr^{-1}, leaving little room for a net contribution to the global sea-level trend from other sources. Only for the PGS predictions P1 to P3, c attains larger values, allowing for a net contribution from a combined effect of the glaciers and the terrestrial hydrosphere.

The regression coefficients β and γ for the PGS predictions and the steric sea-level heights, respectively, are given in table 7. Using I500 as the steric model, β varies from 0.44 for P1 to 1.40 for P7, while all β values are approximately 15% larger for regressions using L500 and L3000 instead of I500.

The regression coefficient γ for the steric dataset L3000 has a value of approximately 0.3–0.45, indicating that these predictions of steric heights overestimate the signal as seen by the tide gauges by a factor larger than 2. For L500, γ is always close to the ideal value of 1.0, which is equivalent to L500 reproducing the steric signal seen at the tide gauges very well. I500 seems to underestimate the steric contribution on the regression grid and γ turns out to be of the order of 1.2–1.3.

In table 8, results of the regression analysis for selected combinations of fingerprints are given. The results confirm the discussion of tables 6 and 7 with respect to the steric and PGS. For all solutions presented in table 8, the steric signal based on I500, L500 and L3000 contributes to the averages on the regression grids of the order of 0.10, 0.20 and 0.15 mm yr^{-1}, respectively. For the

Table 8. Selected results of the regression analysis. (Column M (model) gives the factors included in the regression function (4.1). The symbols used to denote the columns are the same as in table 5, and for each regression model, the two lines have the same meaning as explained in that table. All quantities in mm yr^{-1}, except for V, which is in %. The two models given in bold are those shown in figure 5. A table of the complete results for all model combinations is available at http://www.sbl.statkart.no/projects/pgs/analyses/.)

M	α_A	α_G	β	γ	c	E_{mod}	V
A,G,L500,c	1.14±0.36	0.06±0.02		0.21±0.04	−0.28±0.38	1.14	10.86
	0.50±0.16	0.14±0.05		0.22±0.04	−0.28±0.38	0.59	
G,L500,c		0.03±0.02		0.22±0.04	0.87±0.12	1.12	10.02
		0.06±0.04		0.22±0.04	0.87±0.12	1.16	
A,G,P1,c	0.54±0.29	0.02±0.01	−0.19±0.02		0.65±0.31	1.01	11.11
	0.24±0.13	0.11±0.06	−0.05±0.01		0.65±0.31	0.95	
A,G,P7,c	1.15±0.28	0.01±0.01	−0.40±0.03		0.27±0.30	1.02	13.49
	0.50±0.12	0.06±0.06	−0.08±0.01		0.27±0.30	0.75	
G,P1,c		0.01±0.01	−0.20±0.02		1.20±0.10	1.01	10.81
		0.07±0.06	−0.05±0.01		1.20±0.10	1.21	
G,P7,c		0.00±0.01	−0.41±0.03		1.42±0.10	1.01	12.77
		−0.02±0.01	−0.08±0.01		1.42±0.10	1.32	
A,G,P1,I500,c	0.69±0.37	0.06±0.03	−0.07±0.02	0.09±0.02	0.33±0.40	1.10	12.21
	0.31±0.17	0.13±0.06	−0.03±0.01	0.06±0.01	0.33±0.40	0.79	
A,G,P2,I500,c	0.61±0.37	0.04±0.03	−0.09±0.02	0.08±0.02	0.46±0.40	1.10	13.10
	0.27±0.16	0.09±0.07	−0.04±0.01	0.06±0.02	0.46±0.40	0.83	
A,G,P7,I500,c	1.16±0.35	0.04±0.03	−0.19±0.04	0.08±0.02	0.01±0.38	1.10	12.89
	0.52±0.16	0.09±0.07	−0.06±0.01	0.06±0.02	0.01±0.38	0.61	
A,G,P1,L500,c	0.63±0.37	0.04±0.02	−0.09±0.02	0.22±0.04	0.35±0.40	1.14	12.74
	0.28±0.16	0.09±0.04	−0.04±0.01	0.22±0.04	0.35±0.40	0.90	
A,G,P2,L500,c	0.54±0.37	0.02±0.02	−0.12±0.02	0.20±0.04	0.50±0.40	1.14	13.79
	0.24±0.16	0.05±0.05	−0.05±0.01	0.20±0.04	0.50±0.40	0.94	
A,G,P7,L500,c	1.18±0.36	0.02±0.02	−0.22±0.04	0.20±0.04	−0.03±0.38	1.15	13.37
	0.52±0.16	0.06±0.05	−0.06±0.01	0.20±0.04	−0.03±0.38	0.69	
A,G,P1,L3000,c	0.49±0.37	0.04±0.02	−0.09±0.02	0.15±0.04	0.51±0.39	1.11	11.24
	0.22±0.16	0.09±0.04	−0.04±0.01	0.15±0.04	0.51±0.39	0.93	
A,G,P2,L3000,c	0.41±0.37	0.02±0.02	−0.12±0.02	0.14±0.04	0.65±0.40	1.10	12.43
	0.18±0.16	0.05±0.05	−0.05±0.01	0.14±0.04	0.65±0.40	0.97	
A,G,P7,L3000,c	1.06±0.36	0.03±0.02	−0.22±0.04	0.13±0.04	0.11±0.38	1.11	11.77
	0.47±0.16	0.06±0.04	−0.06±0.01	0.13±0.04	0.11±0.38	0.71	
G,P1,L500,c		0.02±0.02	−0.10±0.02	0.22±0.04	0.99±0.12	1.13	12.41
		0.05±0.05	−0.04±0.01	0.22±0.04	0.99±0.12	1.22	
G,P7,L500,c		−0.01±0.02	−0.22±0.04	0.21±0.04	1.15±0.13	1.13	12.65
		−0.02±0.02	−0.06±0.01	0.21±0.04	1.15±0.13	1.28	

complete grids, these contributions are nearly the same for L500 and L3000, while for I500 the 'global' values are smaller and of the order of 0.06 mm yr^{-1}. The 95% uncertainties are for all three models less than 0.05 mm yr^{-1}. For the L500 dataset, the explained fraction of the variance is the highest. Moreover, the regression coefficient for the L500 dataset is close to 1 (see table 7). Therefore, the steric contribution computed on the basis of this dataset appears to be most consistent with the spatial pattern of the local sea-level trends observed by the

tide gauges. For L500, the steric contribution to global sea-level rise appears to be of the order of 0.22 ± 0.04 mm yr^{-1}, independent of which PGS model is used. However, while L500 may best represent the steric contribution at the tide gauges, which are mostly at coastal locations, L3000 is more appropriate in the open ocean. The global average of L3000 is 0.35 mm yr^{-1}, compared to 0.21 mm yr^{-1} for L500 (see table 3). Therefore, the value of 0.22 ± 0.04 mm yr^{-1} obtained here for the L500 dataset has to be considered as a lower limit for the steric contribution to global sea-level rise rather than its true value.

The largest uncertainty for the contributions from the two ice sheets included here results from uncertainties in the PGS model, which affects particularly the Antarctic ice sheet contribution. For any given PGS model, the Antarctic and Greenland ice sheet contributions are largest for the models using I500 and smallest for L500. Based on the full regression models, the best estimates for the contribution of the Antarctic and Greenland ice sheets to the global sea-level trend are 0.4 ± 0.2 and 0.10 ± 0.05 mm yr^{-1}.

Including only the fingerprints of the two large ice sheets in the regression model results in very large melting trends for both ice sheets (not given in the table). These trends are considerably reduced if a steric fingerprint is included and, even more so, if the PGS fingerprint is also added to the regression model.

The regression results for the Antarctic ice sheet are those depending most on the selected PGS model, thus indicating that any error in the PGS model will affect the regression coefficient for the Antarctic ice sheet. Moreover, the Antarctic rates also affect the constant c due to the deficiencies in the spatial distribution of the tide gauges. Therefore, in table 8, regression results are included for models where the Antarctic fingerprint has been omitted. For almost all of these models, the Greenland ice sheet results are no longer significant, and the constant c absorbs most of the average on the regression grids. This is a strong indication that the Antarctic fingerprint is crucial in explaining the spatial pattern of the RSL trends as deduced from the tide gauge network. However, omitting the Antarctic fingerprint from the regression also affects the regression coefficient for the PGS (see table 7).

In figure 5, the extrapolation of two regression models to the complete steric grid is shown. Both use the PGS prediction P2. The model based on L500 shows the larger spatial variability induced by the steric data. Both models show a largely negative sea-level trend for high southern latitudes arising mainly from a combination of the PGS (see figure 3) and the geoid changes and elastic response of the solid Earth to the present-day deloading of the Antarctic ice sheet. A small negative steric contribution in the circum-Antarctic (see figure 1) further increases the negative sea-level trends in this region. On the Northern Hemisphere, the pattern is a combination of a rise due to added water from the Antarctic ice sheet and the steric rise due to warming, superimposed by land uplift due to post-glacial rebound and the geoid and elastic response due to more local deloading of the Greenland ice sheet.

Restricted to the regression grid, the two models have average sea-level rise of 1.14 ± 0.85 and 1.10 ± 0.84 mm yr^{-1} for the L500 and I500 steric data, respectively. The errors given are maximum standard errors. These values fall well into the range of sea-level rise of 1–2 mm yr^{-1} widely quoted for the rise over the last 100 years. However, the average values for the complete grid are

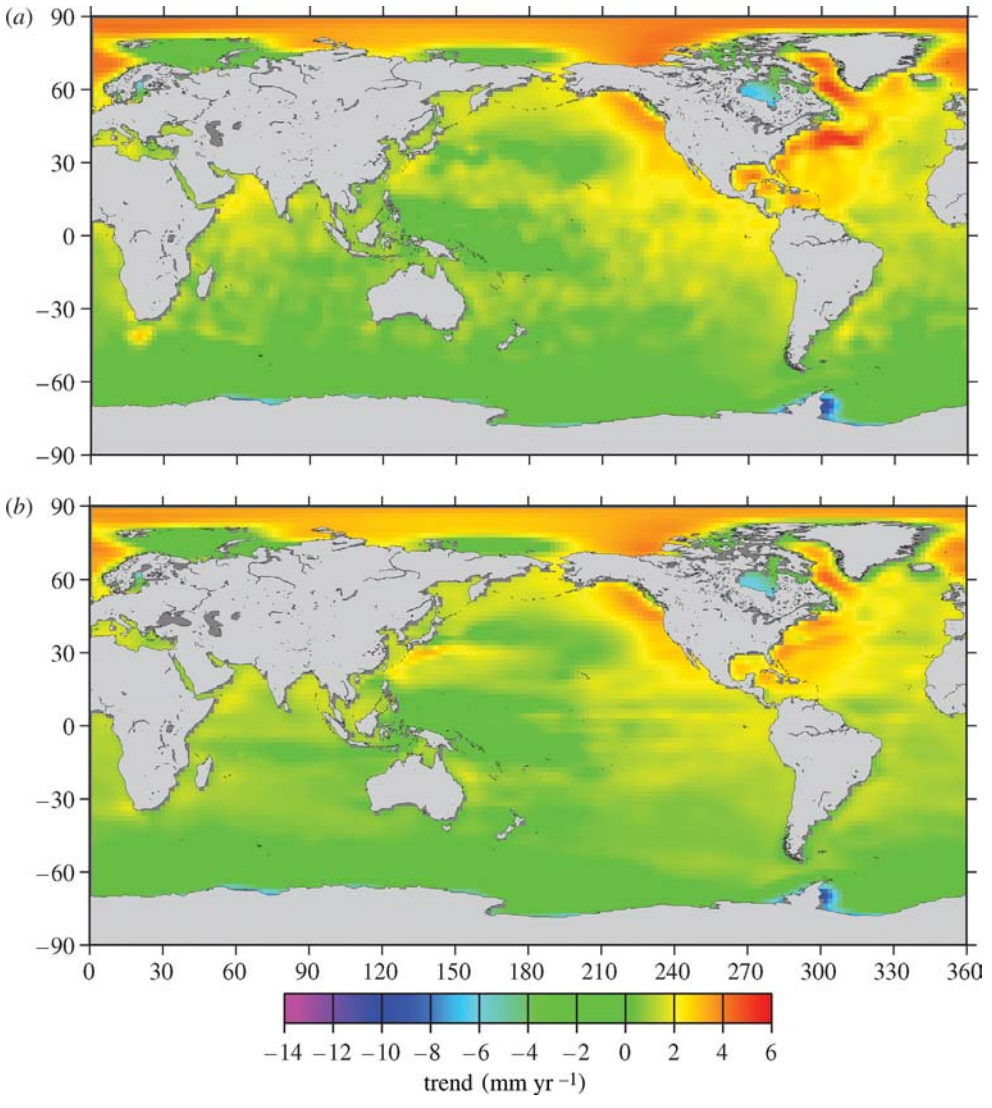

Figure 5. Global model of local sea-level trends in the time window 1950–2000. (*a*) Model A,G,P2,L500,c; (*b*) model A,G,P2,I500,c (both models indicated in bold in table 8). Global sea-level rise is (*a*) 0.94 ± 0.76 and (*b*) $0.83 \pm 0.72\,\mathrm{mm\,yr^{-1}}$. See text for a discussion of the uncertainties.

0.94 ± 0.76 and $0.83 \pm 0.72\,\mathrm{mm\,yr^{-1}}$, respectively. It has to be emphasized here that these values are for a sea-level rise with respect to the solid Earth surface. No correction has been made for vertical motion of the ocean bottom due to tectonics, sedimentation or subsidence caused by human activity.

The global values are lower than the values obtained for the regression grid, and they are at the very low end of values generally reported for the global sea-level rise over the last 50–100 years. The basic assumptions for the extrapolation of the models from the regression grid to the global grid are: (i) the regression model is appropriately representing the long spatial wavelength in sea-level

trends and (ii) there are no other open ocean contributions to global sea-level rise not sensed by the tide gauges. As discussed above, the results for the steric contributions using the L500 and I500 datasets are likely to be minimum estimates. The comparison with the global average of the L3000 dataset indicates that the actual steric contribution may be 0.1–0.2 mm yr^{-1} larger. Therefore, a global sea-level rise value of 1.05 ± 0.75 mm yr^{-1} is considered to be more likely. The other main uncertainty arises from the assumption that the value of the constant c obtained for the regression grid can be used for the global ocean to represent the contributions from the factors not included in the regression (see §2). Without detailed models for these factors, the validity of this second assumption can hardly be assessed.

The spatial correlation coefficient for the two models shown in figure 5 with the observed RSL trends are 0.36 and 0.35, respectively. In general, the solutions for the full regression model (4.1) result in correlations with the observations of the order of 0.30–0.45. The highly significant correlation between model and observation indicates that the model very well approximates the longer spatial wavelength in the observed sea-level trends.

6. Conclusions

A regression model consisting of the fingerprints of PGS, steric sea-level changes and ice mass changes over Antarctica and Greenland explains of the order of 10–15% of the variance of the observed RSL trends. The resulting regression models are correlated with the observations with the correlation coefficient being of the order of 0.40, which indicates that the model represents the large-scale pattern in the observed trends well. The low fraction of variance explained by the models is due to the considerable spatial variance in the RSL trends caused by factors with small and intermediate spatial scales (including but not limited to tectonic vertical land motion, atmospheric circulation changes and unmodelled steric changes, see §2).

The regression results presented and discussed in §5 show that the observed spatial pattern of the RSL trends is compatible with a contribution from the melting of the Greenland ice sheet of 0.05–0.15 mm yr^{-1}, and a contribution of the Antarctic ice sheet of 0.27–0.50 mm yr^{-1}. The uncertainties attached to these numbers are of the order of 0.07 and 0.2 mm yr^{-1}, respectively. Based on the regression results, the steric contribution to global sea-level rise is likely to be at least 0.20 ± 0.04 mm yr^{-1}.

The steric contribution over the open ocean is likely to be larger than what is predicted for the tide gauge locations on the basis of oceanographic observations. Therefore, the actual steric contribution to global sea-level rise is estimated to be closer to 0.35 ± 0.1 mm yr^{-1}. This value is in agreement with previous estimates by, for example, Lombard *et al.* (2005) and falls into the range of values discussed in the IPCC assessment (Church *et al.* 2001).

The contributions of both the Antarctic and Greenland ice sheets determined here fall well into the uncertainty limits of the mass balance of these ice sheets discussed in Warrick *et al.* (1996) and Church *et al.* (2001). However, the results reported here assign a high significance to the fact that both ice sheets have

contributed mass to the ocean and thus seem to narrow down the uncertainties discussed in the IPCC assessments.

For most models, the part of the average RSL trend not explained by the factors in the regression analyses is of the order of $0.5 \pm 0.4\,\mathrm{mm\,yr^{-1}}$. The extrapolation of this value onto the global ocean is a major uncertainty. Nevertheless, this remaining average contribution is consistent with mass balances for glaciers and the terrestrial hydrosphere as reviewed in, for example, Church *et al.* (2001).

Potential biases of the regression results and particularly the extrapolation to the global ocean surface can result from (i) long-term changes in the Greenland and Antarctic ice sheets, which would introduce a visco-elastic response highly correlated with the elastic fingerprints used here, (ii) errors in the PGS predictions, which most likely would affect the results for the Antarctic ice sheet strongly and (iii) unaccounted factors with fingerprints having large spatial variations. These potential biases warrant further studies. Nevertheless, the relatively high stability of the regression results over a wide range of models and predictions underlines the potential of the fingerprint method. Moreover, it indicates that the uncertainty estimates are realistic.

In summary, the average sea-level rise as seen by the global tide gauge network is consistent with (i) a positive contribution from the two large ice sheets, (ii) a negative contribution of PGS (though only on the tide gauge network; averaged over the total surface of the ocean, the PGS must have zero contribution to sea-level rise), (iii) a positive contribution from steric changes and (iv) an unexplained part, most likely due to glaciers and terrestrial hydrosphere. For the part of the ocean covered by tide gauges, the sum of these contributions amounts to $1.10 \pm 0.85\,\mathrm{mm\,yr^{-1}}$. Extrapolating the regression results to the complete steric grid, the most likely result for the global sea-level rise is found to be $1.05 \pm 0.75\,\mathrm{mm\,yr^{-1}}$.

The results presented here demonstrate the potential of the fingerprint method to extract useful information from the sea-level observations provided by the global network of tide gauges. The model set up here explains only a small fraction of the total variance of the observed sea-level trends, keeping the statistical significance of the results low. In order to improve the model, other forcing factors need to be included, in particular, continental glaciers, terrestrial hydrosphere and atmospheric forcing. Most records only cover part of the time interval considered here, and this is best taken into account by setting up the regression model for time-series of monthly or annual means instead of local trends. On the observational side, additional sea-level observations, particularly from high-latitude locations, would help to improve the model. Ultimately, combining tide gauge observations with satellite altimetry and other observations such as Earth rotation, gravity variations and vertical land motion to constrain a self-consistent model based on consistent fingerprints of the forcing factors will make best use of the available information.

The post-glacial rebound signal was computed from datasets provided by J. X. Mitrovica. The tide gauge data were taken from the database maintained by the Permanent Service for Mean Sea Level. The steric sea-level changes computed from the Levitus and Ishii datasets were kindly provided by Anny Cazenave. The author would like to thank these persons for their valuable support. Without their help and, in particular, without the long-lasting work of the PSMSL, this

study would not have been possible. The author would like to thank the reviewers C. K. Shum, Philip Woodworth and Bruce Douglas as well as an anonymous referee for their very thoughtful comments, which helped to improve the original manuscript considerably. Part of this work was supported by a NASA grant in the frame of the Interdisciplinary Science Program.

References

Barnett, T. P. 1984 The estimation of "global" sea level change: a problem of uniqueness. *J. Geophys. Res.* **89**, 7980–7988.

Chelton, D. B. & Enfield, D. B. 1986 Ocean signals in tide gauge records. *J. Geophys. Res.* **91**, 9081–9098.

Church, J. A., Gregory, J. M., Huybrechts, P., Kuhn, M., Lambeck, K., Nhuan, M. T., Qin, D. & Woodworth, P. L. 2001 Changes in sea level. In *Climate change 2001: the scientific basis. Contribution of Working Group I to the Third Assessment Report of the Intergovernmental Panel on Climate Change* (ed. J. T. Houghton, Y. Ding, D. J. Griggs, M. Noguer, P. J. van der Linden, X. Dai, K. Maskell & C. A. Johnson), p. 881. Cambridge, UK: Cambridge University Press.

Douglas, B. C. 1991 Global sea level rise. *J. Geophys. Res.* **96**, 6981–6992.

Douglas, B. C. 1997 Global sea level rise: a redetermination. *Surveys Geophys.* **18**, 279–292. (doi:10.1023/A:1006544227856)

Emery, K. O. & Aubrey, D. G. 1991 *Sea levels, land levels, and tide gauges.* Berlin: Springer.

Farrell, W. E. & Clark, J. A. 1976 On postglacial sea level. *Geophys. J. R. Astron. Soc.* **46**, 647–667.

Gornitz, V. & Lebedeff, S. 1987 Global sea level changes during the past century. In *Sea level fluctuations and coastal evolution*, vol. 41 of Special Publications (ed. D. Nummedal, O. H. Pilkey & J. D. Howard), pp. 3–16. Tulsa, OK: Society of Economic Paleontologists and Mineralogists.

Gröger, M. & Plag, H.-P. 1993 Estimations of a global sea level trend: limitations from the structure of the PSMSL global sea level data set. *Global Planet. Change* **8**, 161–179. (doi:10.1016/0921-8181(93)90023-H)

Houghton, J. T., Meira Filho, L. G., Callander, B. A., Harris, N., Kattenberg, A. & Maskell, K. (eds) 1996 *Climate change 1995—the science of climate change.* Cambridge, UK: Cambridge University Press.

Houghton, J. T., Ding, Y., Griggs, D. J., Noguer, M., van der Linden, P. J., Dai, X., Maskell, K. & Johnson, C. A. (eds) 2001 *Climate change 2001: the scientific basis. Contribution of Working Group I to the Third Assessment Report of the Intergovernmental Panel on Climate Change.* Cambridge, UK: Cambridge University Press.

Ishii, M., Kimoto, M. & Kachi, M. 2003 Historical ocean subsurface temperature analysis with error estimates. *Mon. Weather Rev.* **131**, 51–73. (doi:10.1175/1520-0493(2003)131<0051:HOSTAW>2.0.CO;2)

Lambeck, K. 1993 Glacial rebound of the British Isles—I. Preliminary model results, II. A high-resolution, high precision model. *Geophys. J. Int.* **115**, 941–990.

Levitus, S., Stephens, C., Antonov, J. & Boyer, T. 2000 *Yearly and year-season upper ocean temperature anomaly field, 1948–1998.* Washington, DC: Technical report, US Government Printing Office.

Lombard, A., Cazenave, A., Le Traon, P.-Y. & Ishii, M. 2005 Contribution of thermal expansion to present-day sea level change revisited. *Global Planet. Change* **47**, 1–16. (doi:10.1016/j.gloplacha.2004.11.016)

Meier, M. F. 1984 Contribution of glaciers to global sea level. *Science* **226**, 1418–1421.

Milne, G. A., Mitrovica, J. X. & Davis, J. L. 1999 Near-field hydro-isostasy: the implementation of a revised sea-level equation. *Geophys. J. Int.* **139**, 464–482. (doi:10.1046/j.1365-246x.1999.00971.x)

Mitrovica, J. X., Tamisiea, M. E., Davis, J. L. & Milne, G. A. 2001 Recent mass balance of polar ice sheets inferred from patterns of global sea-level change. *Nature* **409**, 1026–1028. (doi:10.1038/35059054)

Peltier, W. R. 1998 Postglacial variations in the level of the sea: implications for climate dynamics and solid-earth geophysics. *Rev. Geophys.* **36**, 603–689. (doi:10.1029/98RG02638)

Peltier, W. R. & Tushingham, A. M. 1991 Influence of glacial isostatic adjustment on tide gauge measurements of secular sea level change. *J. Geophys. Res.* **96**, 6779–6796.

Pirazzoli, P. A. 1989 Present and near-future global sea-level changes. *Palaeogeogr. Palaeoclimatol. Palaeoecol.* **75**, 241–258. (doi:10.1016/0031-0182(89)90189-2)

Plag, H.-P. 1993 The "sea level rise" problem: an assessment of methods and data. In *Proc. Int. Coastal Congress, Kiel 1992*, pp. 714–732. Frankfurt: P. Lang Verlag.

Plag, H.-P. & Jüttner, H.-U. 2001 Inversion of global tide gauge data for present-day ice load changes. In *Proc. Second Int. Symp. on Environmental Research in the Arctic and Fifth Ny-Ålesund Scientific Seminar* (ed. T. Yamanouchi). Special Issue, No. 54 in Memoirs of the National Institute of Polar Research.

Plag, H.-P., van Dam, T., Blewitt, G. & Kierulf, H. P. 2005 A proposal for a consistent model of air pressure loading as part of the International Terrestrial Reference System (ITRS) Conventions. *Geophys. Res. Abstr.* **7**, EGU05-A-10113.

Quinlan, G. & Beaumont, C. 1982 The deglaciation of Atlantic Canada as reconstructed from the post glacial relative sea-level record. *Can. J. Earth Sci.* **19**, 2232–2246.

Warrick, R. A., Provost, C. L., Meier, M. F., Oerlemans, J. & Woodworth, P. L. 1996 Changes in sea level. In *Climate change 1995—the science of climate change* (ed. J. T. Houghton, L. G. Meira Filho, B. A. Callander, N. Harris, A. Kattenberg & K. Maskell), pp. 359–405. Cambridge, UK: Cambridge University Press.

Woodworth, P. & Player, R. 2003 The permanent service for mean sea level: an update to the 21st century. *J. Coastal Res.* **19**, 287–295.

Woodworth, P. L., Spencer, N. E. & Alcock, G. 1990 On the availability of European mean sea-level data. *Int. Hydrogr. Rev.* **LXVII**, 131–146.